

Deposition of p-Type Microcrystalline Silicon Film and Its Application in Microcrystalline Silicon Solar Cells*

Chen Yongsheng^{1,2,†}, Yang Shi'e¹, Wang Jianhua³, Lu Jingxiao¹, Gao Xiaoyong¹,
Gu Jinhua¹, Zheng Wen¹, and Zhao Shangli¹

(1 Key Laboratory of Material Physics, Department of Physics, Zhengzhou University, Zhengzhou 450052, China)

(2 Institute of Plasma Physics, Chinese Academy of Sciences, Hefei 230031, China)

(3 Department of Materials Science and Engineering, Wuhan Institute of Technology, Wuhan 430073, China)

Abstract: Highly conductive boron-doped hydrogenated microcrystalline silicon ($\mu\text{c-Si:H}$) films and solar cells are prepared by plasma enhanced chemical vapour deposition (PECVD). The effects of diborane concentration, thickness and substrate temperature on the growth and properties of B-doped layers and the performance of solar cells with high deposited rate i-layers are investigated. With the optimum p-layer deposition parameters, a higher efficiency of 5.5% is obtained with 0.78nm/s deposited i-layers. In addition, the carriers transport mechanism of p-type $\mu\text{c-Si:H}$ films is discussed.

Key words: boron-doped $\mu\text{c-Si:H}$ films; Raman crystallinity; dark conductivity; solar cells

PACC: 7280N; 7830G; 8115H

CLC number: TN305.92

Document code: A

Article ID: 0253-4177(2008)11-2130-06

1 Introduction

P-type layers are very important to the performance of silicon thin film solar cells^[1,2]. In order to achieve a perfect-performance solar cell, p-layers must have high optical transmittance and high conductivity. A p-type $\mu\text{c-Si:H}$ layer can be considered to be "good" if its Raman crystallinity is larger than 0.5 and the corresponding dark conductivity (σ_d) at room temperature is above $1\Omega^{-1} \cdot \text{cm}^{-1}$ for a thickness of 20~30nm. In practice, even thinner $\mu\text{c-Si:H}$ p-type window layers are used within solar cells due to the need for high transparency. Previous studies have indicated that boron-doped $\mu\text{c-Si:H}$ films are attractive alternative in the sense of their high doping efficiency, high electrical conductivity, and low optical absorption. This type of material has now been used in solar cells to improve the photovoltaic performance^[1,3]. Due to the low thermal stability of diborane (B_2H_6), the properties of p-doped $\mu\text{c-Si:H}$ films are very sensitive to the deposition parameters, and the doped mechanism remains unclear.

In this paper, we present the structural and electrical properties of boron-doped p-type $\mu\text{c-Si:H}$ films deposited at different process parameters and its influence on the performance of $\mu\text{c-Si:H}$ film solar cells.

2 Experiment

Boron-doped microcrystalline layers were grown on quartz glass and SnO_2/ZnO films coated glass by conventional RF PECVD technique (13.56MHz) in a separate chamber in the same cluster tool system using diborane (diluted to 0.1% in H_2) as dopant gas to prepare p-type materials. The silane and diborane concentrations are defined as $C_{\text{Si}} = F_{\text{SiH}_4} / (F_{\text{SiH}_4} + F_{\text{H}_2})$ and $C_{\text{B}} = F_{\text{B}_2\text{H}_6} / F_{\text{SiH}_4}$, respectively, where F_{SiH_4} , F_{H_2} , and $F_{\text{B}_2\text{H}_6}$ represent the flow rates of SiH_4 , H_2 and B_2H_6 . The thickness of the p-doped $\mu\text{c-Si:H}$ films was measured by a spectroscopic ellipsometry to be about 200nm. The deposition rate (R_d) was determined by the thickness divided by the deposition time. The p-i-n solar cells were grown on glass substrates coated with SnO_2/ZnO films, and Al layer was evaporated as back contacts. The p-i-n structures consist of a 30nm-thick microcrystalline p-layer, a 1.5 μm -thick microcrystalline i-layer, and a 50nm-thick amorphous n-layer. The doped layers were prepared by RF excitation using phosphine (diluted to 0.1% in H_2) as dopant gas, and the intrinsic layer was prepared by VHF technique at 75MHz. The deposition rate maintains at 0.78nm/s. In order to reduce the effect of p-layer microstructure on the characteristic of i-layer, H_2 plasma treatment for different times was used before the deposition

* Project supported by the State Key Development Program for Basic Research of China (No. 2006CB202601) and the Basic Research Project of Henan Province (No. 072300410140)

† Corresponding author. Email: chysh2003@zzu.edu.cn

Received 4 January 2008, revised manuscript received 19 July 2008

Table 1 Deposition parameters of boron-doped $\mu\text{c-Si:H}$ films and solar cells T_{sub} is the substrate temperature, P_{w} is the plasma power, and d_{ele} is the electrodes distance.

Film type	$C_{\text{SiH}_4}/\%$	Total flow /sccm	d_{ele}/cm	$T_{\text{sub}}/^\circ\text{C}$	P_{w}/W	Pressure /Torr	$C_{\text{B}}/\%$	$\text{PH}_3/\text{SiH}_4/\%$
p-doped	1	200	2	150	50	2	0.1~1	—
				50~220			0.5	
Intrinsic	4	250	1.5	200	140	2.3	—	—
n-doped	1	200	2	170	50	1	—	0.8

of i-layer to induce nucleation inside the i-layer itself (close to the p/i interface). The main deposition parameters are listed in Table 1.

The dark conductivity on quartz glass was measured at room temperature using coplanar Al contacts. To study the crystallinity of the films on SnO_2/ZnO films coated glass, Raman spectra were measured in a back-scattering configuration using a Raman spectrometer with a He-Ne laser exciting source. 5.0 mW output power and 632.8 nm wavelength were used in the measurements. The crystalline ratio R_c was obtained as^[4]

$$R_c = (I_{520} + I_{510}) / (I_{520} + I_{510} + I_{480})$$

where I_{520} and I_{510} are the intensities of crystalline like peaks whereas I_{480} is that of amorphous like peak of the transverse optic Si-Si vibrations in the Raman spectra^[5,6]. An X-ray diffractometry (XRD) with a $\text{CuK}\alpha$ radiation source was employed to determine the orientations of the crystallites. The grain size, d_c , calculated from the (111) peak using the Scherrer formula^[4], is $d_c = k\lambda / \beta \cos\theta$, where k (taken as 0.9 in our study) is a constant determined by the geometry of the crystallite, λ is the wavelength of the X-ray radiation, and β is the full width of the diffraction angle (2θ) at half-maximum of the diffraction peak. The solar cells were characterized by measuring the current-voltage characteristic under AM 1.5 illumination and the spectral response.

3 Result and discussion

3.1 Effect of diborane concentration

Figure 1 illustrates both the dark conductivity (σ_d) at room temperature and the degree of crystallinity (R_c) in the films as a function of C_B . As C_B increases, the Raman crystallinity decreases monotonously. However, the σ_d increases with C_B at first. The maximum σ_d is about $0.68 \Omega^{-1} \cdot \text{cm}^{-1}$ at $C_B = 0.7\%$. As C_B further increases, the σ_d begins to decrease. The σ_d is determined by the carrier concentration and drift mobility. Increasing C_B would aggrandize the carrier concentration. But the decreasing of crystallinity would reduce drift mobility. So, the σ_d appears a maximum property with C_B . The detailed analysis is

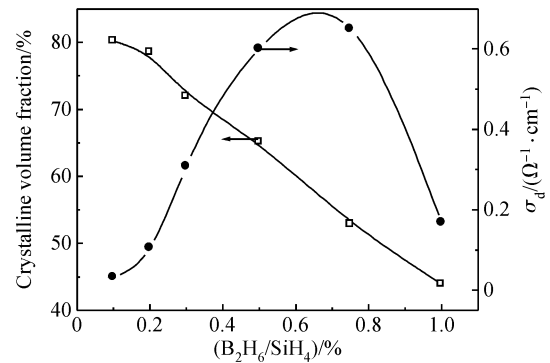


Fig.1 Variations of the crystalline volume fraction and dark conductivity of thin films with diborane concentrations

given later.

Figure 2 shows the X-ray diffraction spectra of samples prepared at different C_B . Diffraction peaks corresponding to the (111), (220) and (311) planes have a preferential orientation of (111). As C_B increases, the intensities of (111) peaks decrease. But the intensities of (220) and (311) peaks increase first and then decrease. The film deposited at $C_B = 0.1\%$ shows the largest intensities and the smallest full width at half-maximum (FWHM) of the diffraction (111) peak, indicating that this sample has the highest volume fraction of crystallinity and the largest grain size. The grain size and deposition rate (R_d) as a function of C_B is shown in Fig. 3, where we can see that the change of the crystalline grain size is consistent with that of R_c .

In order to fabricate p-layers as conductive as possible, it is desirable to obtain highly crystalline p-

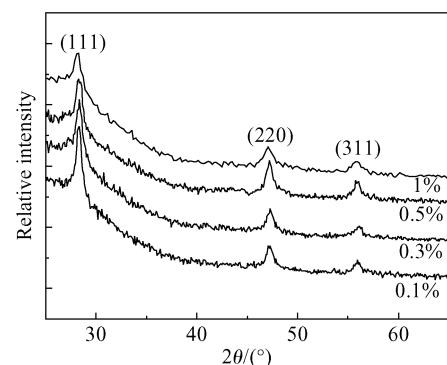


Fig.2 XRD spectra of the boron-doped $\mu\text{c-Si:H}$ films deposited at different diborane concentrations

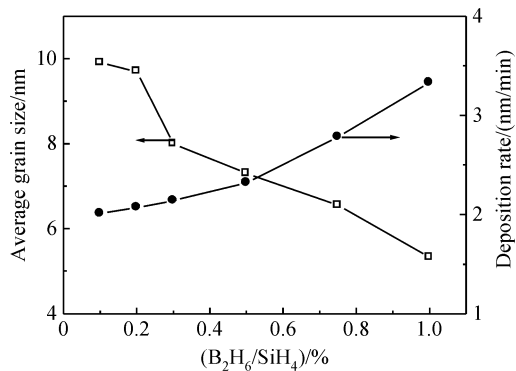


Fig.3 Variations of the grain size and deposition rate with diborane concentration

doped Si:H layers. Figure 4 shows the V_{oc} and J_{sc} of solar cells with the different p-layers deposited under different C_B . As the C_B in p-layer increases, the V_{oc} decreases due to the decrease in Raman crystallinity. The J_{sc} increases as the C_B in p-layer increases and then decreases deeply when C_B in p-layer is above 0.8% due to the decrease of σ_d in p-layer. If the Raman crystallinity factor R_c of the p-layer is too low, i.e. if the p-layer is too amorphous, it will lead to a loss in V_{oc} because of the reduced shift in Fermi-level in such layers, and also to the promotion of subsequent growth of an unsatisfactory intrinsic Si:H layer. So, in our situation diborane concentrations of 0.5% is selected in the follow experiment due to synchronous satisfying higher conductivity and higher crystallinity, and maximum solar cell efficiency is obtained at $C_B = 0.5\%$ in the concentration experiment series.

3.2 Effect of substrate temperature

Figure 5 shows the Raman crystallinity and the dark conductivity of samples deposited at different substrate temperatures (T_{sub}). As T_{sub} increases, R_c and σ_d increase gradually and reach a maximum. As T_{sub} further increases, R_c and σ_d decrease. Interesting phenomenon is that the variation of R_c with T_{sub} is not fully consistent with that of σ_d . The maximum σ_d is

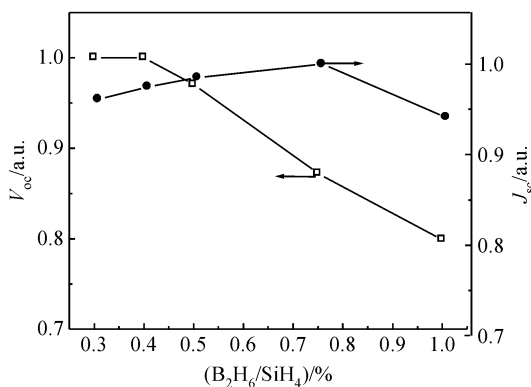


Fig.4 V_{oc} and J_{sc} of solar cells with different p-layers deposited under different diborane concentrations

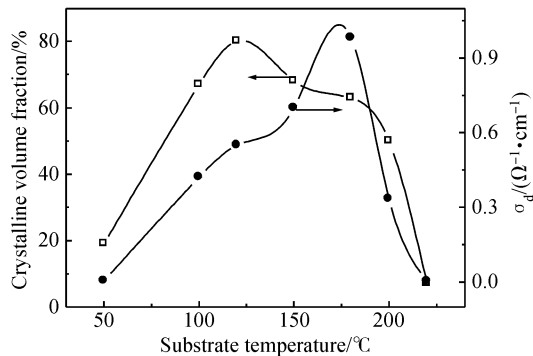


Fig.5 Variations of the crystalline volume fraction and dark conductivity of thin films with substrate temperature

obtained at $T_{sub} = 180^\circ\text{C}$, while the highest crystalline volume fraction of 80% is obtained at $T_{sub} = 120^\circ\text{C}$. The detailed analysis is given later.

Figure 6 shows the X-ray diffraction spectra of samples prepared at different substrate temperatures. Three diffraction peaks corresponding to the (111), (220) and (311) planes have a preferential orientation of (111). As T_{sub} increases, the intensities of these peaks increase first and then decrease, suggesting the change of the microstructure in the film. The film deposited at $T_{sub} = 120^\circ\text{C}$ shows the largest intensities and the smallest FWHM, indicating that this sample has highest crystallinity volume fraction and the largest grain size. The result accords with the R_c . The grain size and deposition rate (R_d) with substrate temperature is shown in Fig. 7, where we can see that the grain size varies from 2.5 to 11.8nm depending on the substrate temperature, and the maximum grain size is obtained at $T_{sub} = 120^\circ\text{C}$.

As one high quality window layer, high conductivity and high conductivity for p-layers is needed. So, the p-layers deposited under $150 \sim 180^\circ\text{C}$ are used to fabricate solar cells. Figure 8 shows the V_{oc} and J_{sc} properties of solar cells with different p-layers deposited under different substrate temperatures. As T_{sub} increases, the V_{oc} of solar cells decreases due to decrease

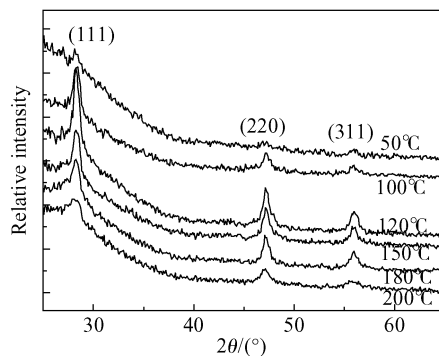


Fig.6 XRD spectra of boron-doped $\mu\text{c-Si:H}$ films with different substrate temperatures

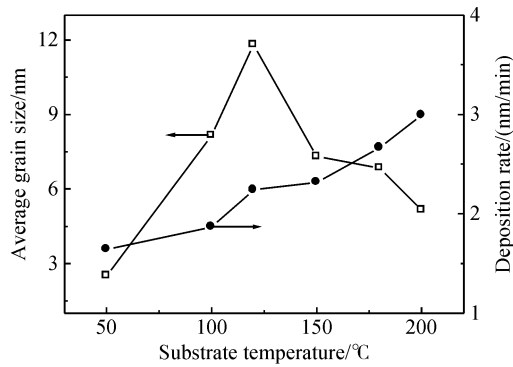


Fig.7 Variations of the grain size and deposition rate with substrate temperature

of crystallinity in p-layers. However, the J_{sc} increases slightly with T_{sub} , which is caused by the increasing of σ_d in p-layer. As a result, a high cell efficiency of p-layer deposited at 150°C is achieved.

3.3 Effect of p-layer thickness

Figure 9 shows the variation of p-layer crystallinity and solar cells properties with the thickness of p-layers. As the p-layer thickness increases, the crystallinity increases deeply and reaches saturation quickly when the thickness is beyond 40nm. The V_{oc} of solar cells increases as the p-layers thickness increases, but the J_{sc} decreases. This is caused by the increase of p-layer crystallinity and the decrease of transparency. The FF and efficiency increase as the p-layer thickness increases first, and then decreases when the p-layer thickness is beyond 30nm. A higher efficiency of 5.5% is obtained.

3.4 Discussion

Microcrystalline is a mixed phase material, containing crystalline grains, grain boundaries (GBs) and amorphous Si network. In brief, we only consider the former two components. At a grain boundary (GB), the crystal lattices of both regions do not match perfectly. The mismatch originates several crystallo-

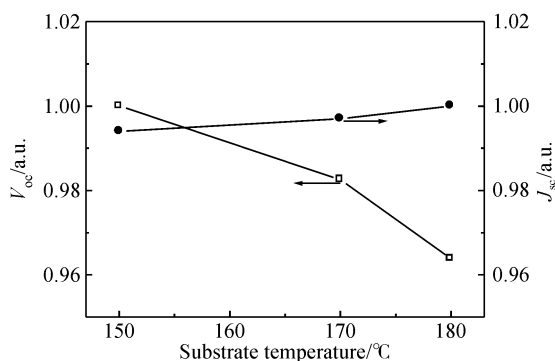


Fig.8 V_{oc} and J_{sc} of solar cells with different p-layers deposited under different substrate temperatures

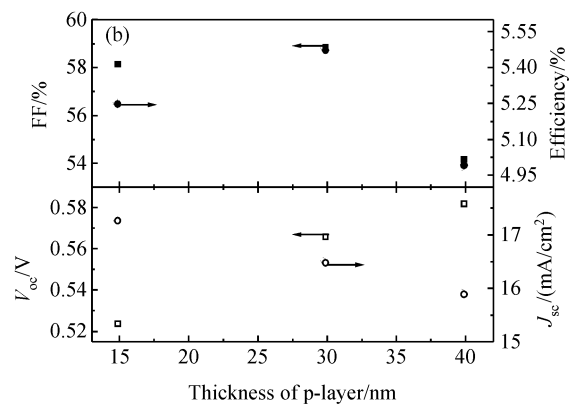
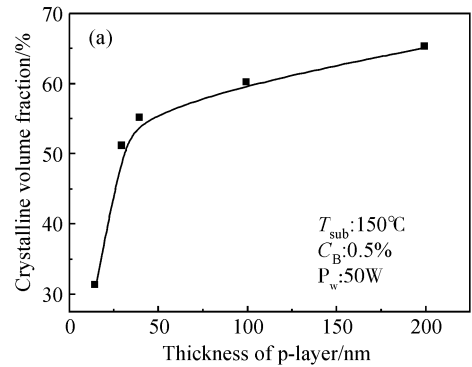


Fig.9 Raman crystallinity of p-layers (a) and the properties of solar cells (b) with the thickness of p-layers

graphic defects, such as vacancies, bended, strained and broken bonds, and dislocations, which constitute the GB. Additionally, impurity atoms tend to diffuse to the GBs to increase the defect density at the grain boundaries^[7]. All these crystallographic imperfections originate electronic defects, which have energy levels in the energy gap of the semiconductor^[7,8]. The defect levels at GBs behave as traps for free carriers. In p-type silicon, the GBs will predominantly trap holes^[9]. So, the trapped carriers build up a positive charge Q_{GB} at the grain boundary.

The charging of the traps at the GB implies a removal of free charges from the grain, leaving space-charge regions (SCRs) near the GBs. Figure 10 (a) shows the positive GBs, and the negative SCRs surrounding the GBs in a p-type μc -Si:H film^[10]. The charge neutrality condition establishes the width of the SCR. In the SCR, an electric field bends the energy bands at each side of the GB. Figure 10 (b) shows the band diagram along the line AA'. At the grain boundary, many defect levels at different energies can be seen. Obeying the Fermi-Dirac statistics, all levels above the Fermi energy level E_F are charged positively. The diagram also shows the band bending qV_b , developed along the SCRs.

The transport of carriers from one grain to its neighbor has three stages; the first one is the flow

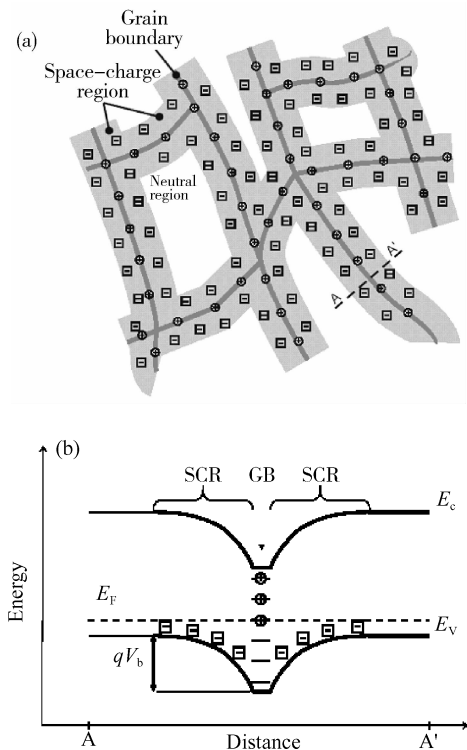


Fig.10 (a) Schematic cross section of a p-type $\mu\text{c-Si:H}$ film, showing charges at the grain boundaries, and the space-charge regions that surround them; (b) Band diagram along the line AA', which contains a grain boundary with its defect levels in the band gap, partially filled with holes

through the neutral part of the grain, secondly through the SCR, and thirdly through the GB. We believe that the electrical transport properties of p-type $\mu\text{c-Si:H}$ film are governed by carrier trapping at the grain boundary. To simplify the model, we assume that $\mu\text{c-Si:H}$ film is composed of identical crystallites with a grain size of g . We further assume that the thickness of the grain boundary is negligible compared to g , and it contains N_t of traps density at the GBs. So, the resistivity ρ in the SCR region is defined as^[10,11]

$$\rho = \frac{1}{q\mu_p p_0} \times \frac{\sqrt{\pi} \operatorname{erfi}(\sqrt{V_b/V_t})}{2\sqrt{V_b/V_t}}$$

where μ_p and p_0 are the mobility and the hole concentration in the grains, and V_t is the thermal voltage (given by $V_t = kT/q$). In $\mu\text{c-Si:H}$ film, the passivation of grain boundary defects can properly take place due to the amorphous silicon content. So, $gN_A > N_t$. The band bending qV_b is independent of grain size, given by^[10,12]

$$qV_b = \frac{q^2 N_t^2}{8\epsilon_0 \epsilon_s N_A}$$

where N_A is the doping concentration in the grain. At high band bending, the ρ increases sharply as V_b increases.

In the diborane concentration experimental se-

ries, the p_0 and N_A increase with the diborane concentration increasing in the plasma, resulting the increasing of σ_d , in despite of μ_p decreases linearity with the decreasing of grain size in p-layer. However, with the further increasing of diborane concentration in the plasma, N_t will increase rapidly due to a mass of B atoms gathered in the GBs. This results in the decreasing of σ_d .

In the substrate temperature series, the increasing of σ_d at low substrate temperature is caused by the increasing of μ_p , which increases with the increasing of R_c . The secondary ion mass spectrometry (SIMS) of samples show that the B atom concentration increases in the film with the increasing of substrate temperature (not shown). So, the higher B atom concentration in the film will generate higher N_t , and results in the decreasing of σ_d combining the decreasing of μ_p , with the further increasing of substrate temperature.

4 Conclusion

The effects of diborane concentration and substrate temperature on the growth and properties of boron-doped $\mu\text{c-Si:H}$ are investigated. Results suggest that the growth rate and the structural and electrical properties of the samples are all strongly dependent on C_B and T_{sub} . In order to deposit p-doped $\mu\text{c-Si:H}$ films with higher R_c and σ_d , it is very important to decrease and passivate the defect in the grain boundaries. The influences of different p-doped $\mu\text{c-Si:H}$ films on the performance of $\mu\text{c-Si:H}$ solar cells are investigated also. Results show that the V_{oc} decreases due to the decreasing of Raman crystallinity and the J_{sc} increases with the increasing of σ_d in p-doped $\mu\text{c-Si:H}$ film. In order to improve the efficiency of solar cells, it is desirable to obtain highly crystalline p-doped Si:H layers with higher conductive and thinner thickness.

References

- [1] Guha S, Yang J, Nath P, et al. Enhancement of open circuit voltage in high efficiency amorphous silicon alloy solar cells. Appl Phys Lett, 1986, 49: 218
- [2] Ferreira G M, Chen C, Koval R J, et al. Optimization of proto-crystalline silicon p-type layers for amorphous silicon n-i-p solar cells. J Non-Cryst Solids, 2004, 338~340: 694
- [3] Kondo M, Nasuno Y, Mase H, et al. Low-temperature fabrication of microcrystalline silicon and its application to solar cells. J Non-Cryst Solids, 2002, 299~302: 108
- [4] Findeisen E, Feidenhans E R, Vigild M E, et al. Hydrogen concentration and mass density of diamondlike carbon films obtained by X-ray and neutron reflectivity. J Appl Phys, 1994, 76: 4636
- [5] Kaneko T, Wakagi M, Onisawa K, et al. Change in crystalline morphologies of polycrystalline silicon films prepared by radio-frequency plasma-enhanced chemical vapor deposition using SiF_4

- + H₂ gas mixture at 350°C. *Appl Phys Lett*, 1994, 64: 1865
- [6] He Y, Wei Y, Zheng G, et al. An exploratory study of the conduction mechanism of hydrogenated nanocrystalline silicon films. *J Appl Phys*, 1997, 82: 3408
- [7] Werner J H, Queisser H J. Electrical and electronic properties of grain boundaries in silicon. *Mat Res Soc Symp Proc*, 1988, 106: 53
- [8] Rhoderick E H, Williams R H. *Metal-semiconductor contacts*. Oxford: Oxford University Press, 1988
- [9] Werner J H, Christensen N E. *Polycrystalline semiconductors II*. In: Werner J H, Strunk H P, ed. *Springer Proceedings in Physics*, Vol. 54. Heidelberg, Germany: Springer, 1991: 145
- [10] Taretto K R. Modeling and characterization of polycrystalline silicon for solar cells and microelectronics, doctor thesis. Universität Stuttgart in Stuttgart, German, 2003
- [11] Kim D M, Khondker A N, Ahmed S S, et al. Theory of conduction in polysilicon: drift-diffusion approach in crystalline-amorphous-crystalline semiconductor system—part I: small signal theory. *IEEE Trans Electron Devices*, 1984, ED-31: 480
- [12] Seto J Y W. The electrical properties of polycrystalline silicon films. *J Appl Phys*, 1975, 46: 5247

p 型微晶硅薄膜的沉积及其在微晶硅薄膜太阳能电池中的应用*

陈永生^{1,2,†} 杨仕娥¹ 汪建华³ 卢景霄¹ 郜小勇¹ 谷锦华¹ 郑文¹ 赵尚丽¹

(1 郑州大学物理工程学院 材料物理重点实验室, 郑州 450052)

(2 中国科学院等离子体物理研究所, 合肥 230031)

(3 武汉工程大学材料科学与工程学院, 武汉 430073)

摘要: 采用等离子体化学气相沉积(PECVD)方法制备了硼掺杂微晶硅薄膜和微晶硅薄膜太阳能电池. 研究了乙硼烷含量、p 型膜厚度及沉积温度对硼掺杂薄膜生长特性和高沉积速率的电池性能的影响. 通过对 p 型微晶硅薄膜沉积参数的优化, 在本征层沉积速率为 0.78nm/s 的高沉积速率下, 制备了效率为 5.5% 的单结微晶硅薄膜太阳能电池. 另外, 对 p 型微晶硅薄膜的载流子疏输运机理进行了讨论.

关键词: B 掺杂微晶硅薄膜; 喇曼晶化率; 暗电导; 太阳能电池

PACC: 7280N; 7830G; 8115H

中图分类号: TN305.92 **文献标识码:** A **文章编号:** 0253-4177(2008)11-2130-06

* 国家重点基础研究发展规划(批准号:2006CB202601)及河南省基础研究计划(批准号:072300410140)资助项目

† 通信作者. Email: chysh2003@zzu.edu.cn

2008-01-04 收到, 2008-07-19 定稿